Title

Increased SNR efficiency in velocity selective arterial spin labeling using multiple velocity selective saturation modules (mm-VSASL)

Journal

Magnetic Resonance in Medicine, 74(3)

ISSN

0740-3194

Authors

Guo, Jia

Wong, Eric C

Publication Date

2015-09-01

DOI

10.1002/mrm.25462

Peer reviewed

HHS Public Access

Author manuscript

Magn Reson Med. Author manuscript; available in PMC 2016 September 01.

Published in final edited form as:

Magn Reson Med. 2015 September ; 74(3): 694–705. doi:10.1002/mrm.25462.

Increased SNR Efficiency in Velocity Selective Arterial Spin Labeling using Multiple Velocity Selective Saturation Modules (mm-VSASL)

Jia Guo[1,*] and **Eric C. Wong**[2,3]

[1]Department of Bioengineering, University of California, San Diego, La Jolla, California, USA

[2]Department of Radiology, University of California, San Diego, La Jolla, California, USA

[3]Department of Psychiatry, University of California, San Diego, La Jolla, California, USA

Abstract

Purpose—Velocity-selective arterial spin labeling (VSASL) is theoretically insensitive to transit delay (TD) effects. However, it uses saturation instead of inversion, resulting in compromised signal to noise ratio (SNR). In this study we explore the use of multiple velocity-selective saturation (VSS) modules in VSASL (mm-VSASL) to improve SNR.

Methods—Theoretical SNR efficiency improvement and optimized parameters were calculated from simulations for mm-VSASL. VSASL with two VSS modules (VSASL-2VSS) was implemented to measure cerebral blood flow in vivo, compared with conventional VSASL (VSASL-1VSS), Pulsed ASL and Pseudo-Continuous ASL. TDs and bolus durations (BDs) were measured to validate the simulations and to examine the TD sensitivity of these preparations.

Results—Compared with VSASL-1VSS, VSASL-2VSS achieved a significant improvement of SNR (22.1 ± 1.9%, $P = 1.7 \times 10^{-6}$) in vivo, consistent with a 22.7% improvement predicted from simulations. The SNR was comparable to or higher (in GM, $P = 4.3 \times 10^{-3}$) than that using PCASL. VSASL was experimentally verified to have minimal TD effects.

Conclusion—Utilizing multiple VSS modules can improve the SNR efficiency of VSASL. Mm-VSASL may result in an SNR that is comparable to or even higher than that of PCASL in applications where long PLDs are required.

Keywords

Velocity-Selective ASL; Arterial Spin Labeling; Velocity-Selective Saturation; Transit Delay; Perfusion

Introduction

In arterial spin labeling (ASL), magnetically labeled water in arterial blood is employed as an endogenous contrast agent to measure local tissue perfusion. In conventional ASL (1-6), it is required to have a spatial gap between the labeling and imaging regions to avoid any

[*]**Correspondence to:** UCSD Center for Functional MRI 9500 Gilman Drive, MC 0677 La Jolla, CA 92093-0677 jguo@ucsd.edu.

undesired perturbation of the tissue magnetization. This gap results in a transit delay (TD) for the labeled blood to reach the destination tissue and a necessary wait time before perfusion-weighted images can be acquired. Due to the complex vasculature and the distribution of arterial blood velocities, the TDs are heterogeneous and are the main source of error in local cerebral blood flow (CBF) quantification (7-9), especially in cases where slow or collateral flow conditions exist (10-13). To tackle these problems, Velocity-Selective ASL (VSASL) (14-16) globally labels spins on the basis of flow velocity, eliminating the gap as well as the associated heterogeneous TDs in conventional ASL.

Eliminating the heterogeneous TDs in ASL guarantees that a single optimal post-labeling delay (PLD) is always available to measure perfusion with both accuracy and maximized SNR efficiency (see Methods). This is because: 1) the condition of PLD ≥ TD can be always satisfied, so potential inaccuracy of perfusion quantification due to violation of this condition can be avoided; and 2) TD no longer limits the choice of PLD, so an optimal PLD can be used to maximize the ASL signal, considering both the amount of labeled blood delivered and the signal loss due to longitudinal relaxation. However, due to the saturation-based labeling in VSASL, the labeling efficiency is compromised, resulting in compromised signal to noise ratio (SNR) compared to inversion based labeling methods such as Pseudo-Continuous ASL (PCASL) (6). In this study, we introduce a novel strategy of utilizing multiple Velocity-Selective Saturation (VSS) modules in VSASL (mm-VSASL) to improve SNR efficiency.

Theory

VSASL acquires images under two preparation conditions: label and control. Under the label condition, the arterial blood is labeled by VSS modules consisted of radio frequency (RF) pulses and flow-weighting gradients, and the spins moving above a chosen cutoff velocity (V_c) are saturated. Under the control condition, the VSS modules are applied without the flow-weighting gradients, leaving the spins unperturbed. The difference between the two conditions is a bolus of labeled spins that is moving above the V_c at the time of labeling. After a delay, perfusion-weighted images are acquired with flow-weighting gradients of the same V_c, generating a VSASL signal that consists of blood that has decelerated through V_c. Note that it is essential to match the V_c in the image acquisition and that in the preparation, so that the VSASL signal is directly proportional to the PLD, or equivalently, so that the TD is effectively eliminated (16).

In conventional VSASL (Figs. 1a and 1c), at the time of imaging, the ASL signal is given by (following (16)):

$$S_{1VSS}=e^{-eTE/T_{2a}}\cdot CBF\cdot M_0\cdot\left(1-e^{-\frac{TR-TI}{T_{1a}}}\right)\cdot e^{-\frac{TI}{T_{1a}}}\cdot TI, \quad (1)$$

where *eTE* is the effective echo time (*TE*) of the VSS module, T_{2a} the transverse relaxation time (T_2) of arterial blood, *CBF* the cerebral blood flow under investigation, M_0 the fully relaxed magnetization, *TR* the repetition time, *TI* the interval between the VSS module and the image acquisition, and T_{1a} the longitudinal relaxation time (T_1) of arterial blood. The term *TI* is used here for consistency with previous VSASL literature, but is equivalent to

PLD. Note that the arterial blood signal recovers from zero due to a global saturation applied immediately after image acquisition, whose purpose is to reset the magnetization (16).

Let α represent the saturation efficiency of VSS module (16):

$$\alpha = e^{-eTE/T_{2a}}, \quad (2)$$

and ΔM_z the longitudinal magnetization difference between the label and the control conditions (see Fig. 1c):

$$\Delta M_z = M_0 \cdot \left(1 - e^{-\frac{TR-TI}{T_{1a}}}\right) \cdot e^{-\frac{TI}{T_{1a}}} \quad (3)$$

Eq. 1 then becomes:

$$S_{1VSS} = \alpha \cdot CBF \cdot \Delta M_z \cdot TI. \quad (4)$$

In this study, a novel labeling strategy using multiple VSS modules is proposed to improve the SNR of VSASL, based on two effects: 1) additional VSS modules create larger magnetization difference between the label and the control conditions; 2) additional VSS modules can label the arterial spins that were outside of the scope of RF coil at the application of the first VSS module as they move in later, so the available bolus duration (BD) is effectively increased.

For simplicity, the case of using two VSS modules (Figs. 1b and 1d) is analyzed to demonstrate the SNR gain. Based on the magnetization states at the time of imaging, the spins that contribute to the ASL signal can be categorized into two groups: 1) one that is labeled only by the first VSS module (lab.1 in Fig. 1d), and 2) one that is labeled at least by the second VSS module (lab.2 in Fig. 1d).

For the first group of spins, at the application of the second VSS module, it has decelerated below V_c, and is therefore not labeled by the second VSS module. The magnetization under the label condition follows the dashed lines in Figure 1d. The magnetization difference between the label and the control conditions, ΔM_{z1}, is given by:

$$\Delta M_{z1} = M_0 \cdot \left(1 - e^{-\frac{TR-TI_1-TI_2}{T_{1a}}}\right) \cdot e^{-\frac{TI_1+TI_2}{T_{1a}}}, \quad (5)$$

and the corresponding ASL signal is:

$$S_{2VSS,tag1} = \alpha^2 \cdot CBF \cdot M_0 \cdot \left(1 - e^{-\frac{TR-TI_1-TI_2}{T_{1a}}}\right) \cdot e^{-\frac{TI_1+TI_2}{T_{1a}}} \cdot TI_1 = \alpha^2 \cdot CBF \cdot \Delta M_{z1} \cdot TI_1, \quad (6)$$

where TI_1 is the interval between the application of the first and the second VSS modules, and TI_2 the interval between the second VSS module and the imaging (Fig. 1b). Note that though the magnetization of the first group is not labeled by the second VSS module, it is still affected by the T_2 relaxation during the second VSS module, resulting in the α^2 term.

The second group of spins consists of two subgroups: 1) one that is created only by the second VSS module, i.e., the spins entering the scope of the RF coil after the first VSS module (dot-dashed lines in Fig. 1d); and 2) one that is labeled by both the first and the second VSS modules, i.e., the spins that are labeled by the first VSS module and remain above V_c at the application of the second VSS module, but eventually decelerate below V_c at the time of imaging, whose magnetization follows dashed lines before and dot-dashed lines after the application of the second VSS module in Figure 1d. Let the relative proportions of the two subgroups' boluses be P_1 and P_2 respectively ($P_1 + P_2 = 1$). P_1 can then be estimated using:

$$P_1 = 1 - P_2 \approx \begin{cases} 0 & TI_1 + TI_2 \leq BD \\ 1 - \frac{BD - TI_1}{TI_2} & TI_1 \leq BD < TI_1 + TI_2, \\ 1 & BD < TI_1 \end{cases} \quad (7)$$

where *BD* is the maximal BD created by one VSS module.

The first subgroup is not affected by the global saturation, so the magnetization under the control condition is fully relaxed (not shown in Fig. 1d), and the ASL signal of subgroup 1 is:

$$S_{2VSS,tag\ 2,sub\ 1} = \alpha \cdot CBF \cdot M_0 \cdot e^{-\frac{TI_2}{T_{1a}}} \cdot TI_2 \cdot P_1. \quad (8)$$

The ASL signal of subgroup 2 is:

$$S_{2VSS,tag\ 2,sub\ 2} = \alpha^2 \cdot CBF \cdot M_0 \cdot \left(1 - e^{-\frac{TR - TI_2}{T_{1a}}}\right) \cdot e^{-\frac{TI_2}{T_{1a}}} \cdot TI_2 \cdot P_2. \quad (9)$$

Combining Eqs. [7] and [8], and the fact that $P_1 + P_2 = 1$, the ASL signal of the second group is:

$$\begin{aligned} S_{2VSS,tag\ 2} = S_{2VSS,tag\ 2,sub\ 1} + S_{2VSS,tag\ 2,sub\ 2} &= \alpha^2 \cdot CBF \cdot M_0 \cdot e^{-\frac{TI_2}{T_{1a}}} \cdot TI_2 \cdot \left[\frac{P_1}{\alpha} + P_2 \cdot \left(1 - e^{-\frac{TR - TI_2}{T_{1a}}}\right)\right] \\ &= \alpha^2 \cdot CBF \cdot M_0 \cdot \left(1 - e^{-\frac{TR - TI_2}{T_{1a}}}\right) \cdot e^{-\frac{TI_2}{T_{1a}}} \cdot TI_2 \cdot \left\{1 + P_1 \cdot \left[\frac{1}{\alpha \cdot \left(1 - e^{-\frac{TR - TI_2}{T_{1a}}}\right)} - 1\right]\right\} \\ &= \alpha^2 \cdot CBF \cdot \Delta M_{z2} \cdot TI_2 \cdot \left(1 + P_1'\right), \end{aligned} \quad (10)$$

where ΔM_{z2} is the magnetization difference of the subgroup 2 of the second group:

$$\Delta M_{z2} = M_0 \cdot \left(1 - e^{-\frac{TR - TI_2}{T_{1a}}}\right) \cdot e^{-\frac{TI_2}{T_{1a}}}, \quad (11)$$

and

$$P_1'=P_1\cdot\left[\frac{1}{\alpha\cdot\left(1-e^{-\frac{TR-TI_2}{T_{1a}}}\right)}-1\right]. \quad (12)$$

With properly chosen imaging parameters $TI_{1/2}$ such that $TI_1 + TI_2 \le BD$, $P_1 = 0$ and $P_1'=0$. The total ASL signal generated by two VSS modules then simplifies to:

$$S_{2VSS}=S_{2VSS,tag\ 1}+S_{2VSS,tag\ 2}=\alpha^2\cdot CBF\cdot(\Delta M_{z1}\cdot TI_1+\Delta M_{z2}\cdot TI_2). \quad (13)$$

The contribution of groups 1 and 2 to the total bolus of labeled blood is weighted (and can be adjusted) by TI_1 and TI_2 respectively.

However, as shown in Eqs. 7 and 12, if the condition $TI_1 + TI_2 \le BD$ is not satisfied, then $P_1'>0$, using Eq. 13 may underestimate the SNR gain or overestimate the CBF. In this case, Eq. 13 is recommended to quantify CBF with the imaging parameters and the P_1 value calculated with Eq. 7, given an empirical or measured value of *BD*. In case of unknown BDs, the potential range of CBF overestimation can be estimated by comparing the values obtained by Eqs. 10 and 13, given an assumed range of P_1 values.

The labeling process utilizing three or more VSS modules follows the derivation above. However, for N VSS modules, the labeling efficiency term is αN, and more modules are beneficial only when the SNR gain by application of additional VSS modules is larger than the additional T_2 relaxation during labeling.

Methods

Simulations

To examine the SNR gains by applying multiple VSS modules, the SNR efficiencies of VSASL with 1, 2 or 3 VSS modules (VSASL-1VSS, VSASL-2VSS and VSASL-3VSS respectively) were simulated in MATLAB 2012a (The Mathworks, Nantick, USA). The SNR efficiency is defined as $S_{ASL}/\sqrt{2TR}$, where S_{ASL} is the ASL signal measured in 2 TRs (a pair of label/control acquisitions). For comparison, the SNR efficiencies of PASL and PCASL were also simulated. For all the labeling methods, the maximal SNR efficiency was calculated at each TR (from 1 to 8 s, with a step size of 0.05 s), and then normalized to that of the VSASL-1VSS at TR of 1 s. A T_1 of 1.66 s and a T_2 of 0.15 s were assumed for arterial blood. An imaging time of 0.3 s was assumed.

In VSASL simulations, an eTE of 20 ms ($\alpha \approx 0.88$) and a maximal BD of 2.0 s (compared with an unlimited BD) were used for each VSS module. At each TR, the maximal ASL signal and the SNR efficiency were calculated using Eq. 13 by searching through the available range of TIs. At the optimized point, the potential effect of CBF overestimation using Eq. 13 was simulated with P_1 ranging from 0 to 0.5.

In simulations using PASL and PCASL, scenarios of TDs being 1.5 and 2 s were considered, so the corresponding PLDs of 1.5 and 2 s were used to obtain the maximal SNR efficiency. For PCASL, a TD of 2.5 s was also considered, as this scenario may be relevant in practice (see Discussion). For PASL, a labeling efficiency of 0.97 (9) was used. In PASL and VSASL, the maximal BD is limited by the spatial extent of the transmit RF coil. We have measured a value of 1.3 s for PASL, and a value of 2.0 s for VSASL, and used these for our simulations. For PCASL, a labeling efficiency of 0.80 (6,17) was used, and the BD was assumed to be TR minus the imaging time and the TD.

In Vivo Experiments

All the in vivo scans were carried out on a 3-Tesla GE scanner (Discovery MR750, GE Healthcare, Waukesha, WI, USA) with a commercial 8-channel receive-only head coil under an IRB-approved protocol.

CBF measurements—Seven young, healthy volunteers (6M, 1F, age 33.4 ± 3.8 y/o) were scanned to measure CBF in gray matter (GM) and white matter (WM).

VSASL: VSASL-1VSS and VSASL-2VSS were tested. To minimize erroneous labeling of static tissue from eddy current effects, the symmetric BIR-8 (sym-BIR-8) design (18) was used as the VSS module, where the RF sub-pulses of BIR-8 are evenly spaced with flow-weighting gradient pulses with a ramp time of 0.5 ms and a maximum amplitude of 20 mT/m. A delay of 0.1 ms before and a delay of 2 ms after each gradient pulse were also inserted to further reduce eddy current effects (18). The V_c was 2 cm/s in the S/I direction in both labeling and imaging. The eTE of each VSS module was determined to be 21.4 ms through Bloch simulations with assumed T_1 of 1.66 s and T_2 of 0.15 s for arterial blood.

From the simulations to maximize the SNR efficiencies at the TR of 4.5 s, optimized TIs were determined to be 1.3 s for the VSASL-1VSS scans and TI_1/TI_2 of 1.15/0.82 s for the VSASL-2VSS scans. Given a measured BD value of 2.0 s (see below), the TIs used in the VSASL-2VSS scans satisfied that $TI_1 + TI_2 \leq BD$, so CBF could be quantified using Eq. 13 without bias. To improve the SNR, two global background suppression (BGS) pulses (19) were applied at 1290 ms and 320 ms prior to image acquisition in VSASL-1VSS scans, and 790 ms and 190 ms prior to image acquisition in VSASL-2VSS scans. Another set of VSASL-2VSS data was collected with a modified second VSS module and one BGS pulse at 190 ms prior to image acquisition (VSASL-2VSS-1BGS). This modified VSS module had an additional phase of π on the last BIR sub-pulse to tip down instead of up spins at the end of the module, effectively serving as a combined VSS and BGS module with reduced specific absorption rate (SAR) and SNR loss due to imperfection of the BGS pulse, without compromising the overall BGS efficiency. Alternative implementations include: 1) addition of phase of $\pi/4$ to the 2^{nd}, 3^{rd}, 6^{th} and 7^{th} segments of the BIR-8 pulses; or 2) addition of phase of $3\pi/2$ to the 2^{nd} and 3^{rd} segments; or 3) addition of phase of $3\pi/2$ to the 6^{th} and 7^{th} segments. All these modifications can achieve the same performance with regards to the velocity sensitivity and off-resonance effects, according to Bloch simulation.

Other parameters included: seven 6 mm-thick slices with 6 mm gaps, field of view (FOV) = 220 × 220 mm, spin echo with matched-phase RF pulses (20), TR/TE = 4.5 s/ 17.9 ms, fat

saturation before excitation, spiral readout with a matrix of 64 × 64, 30 pairs of label and control following 2 dummy repetitions, global saturation pulses at the end of image acquisition.

PASL: CBF maps using PASL (PICORE QUIPSS II (5,9)) were collected with the same imaging parameters as in VSASL. Other parameters were: hyperbolic secant inversion pulse, inversion slab thickness = 200 mm, 20 mm gap between labeling and imaging slabs, TI/TI_1 = 2.4 s/0.8 s (PLD = 1.6 s) and two BGS pulses applied at 1190 ms and 310 ms prior to image acquisition, TR/TE and flow crushing gradients matched to that of the VSASL scans to minimize any potential contamination from intravascular signals. Note that the TI was longer than that typically used to ensure a complete delivery of labeled blood and an accurate quantification of CBF.

PCASL: PCASL scans used the following labeling parameters: 375 μs Hamming shaped pulses with a maximal B_1 of 10 μT (a nominal flip angle of 31.1°) and 1 ms spacing, labeling gradients with 16 mT/m amplitude and 0.9 mT/m mean value, 2 s label duration, 2 s PLD, 46.7 ± 2.8 mm (mean ± standard deviation (STD)) gaps between labeling (on a relatively straight part of the internal carotid arteries and vertebral arteries) and imaging slabs, two BGS pulses applied at 1190 ms and 310 ms prior to image acquisition, and TR/TE and flow crushing gradients matched that in the VSASL scans.

For CBF quantification, four reference images were collected to estimate the receive-coil sensitivity map and the conversion factor between MR signal and the amount of arterial blood from fully relaxed cerebrospinal fluid (CSF) signal. High-resolution anatomical images were collected to generate partial volume ratio maps (Fig. 2a) of GM, WM and CSF using AFNI (21), and then were down-sampled (Fig. 2b) to generate GM and WM regions of interest (ROIs, Fig. 2c).

ASL signals were calculated and averaged across repetitions. The signal attenuation from BGS was compensated with an inversion efficiency of 0.97 for each inversion pulse used. Note that because the b-values of the VSS preparations were non-zero in the label condition but zero in the control condition, a diffusion attenuation difference between these two conditions was expected. To avoid CBF overestimation from this cause, the amount of attenuation difference, $_{p_t}Me^{(-b*\mathrm{D}t)}$, was estimated and removed, where p_t is the partial volume fraction of tissue t (GM, WM or CSF), M is the magnetization of the voxel at the time of application of the VSS module, b is the b-value of the VSS module and D_t is the diffusion coefficient of tissue t (8.9×10^{-4} mm^2/s, 7.0×10^{-4} mm^2/s and 2.9×10^{-3} mm^2/s for GM, WM (22) and CSF (23), respectively). Note that the diffusion attenuation correction was applied on each VSS module used. The acquisition time for each slice was accounted in the calculation of the actual TI for each slice and the CBF values were then calculated using a modified dynamic ASL model (24).

Averaged ASL signals and CBF values were calculated across the GM and WM ROIs for each subject. The ASL signal was treated as direct indicator of SNR, as the noise levels were comparable with similar BGS levels. The temporal STDs (tSTDs) of CBF were also

reported. Note that the tSTDs of ASL signal were not reported because they are simply the tSTDs of CBF scaled by an ASL-CBF conversion constant in each subject.

Multi-TI ASL experiments—In order to validate the timing parameters used in mm-VSASL and to verify the TD insensitivity of VSASL, the BDs and TDs using VSASL were measured by collecting ASL data at multiple TIs. For comparison, TDs and BDs using PASL and PCASL were also measured. Five young, healthy volunteers (4M, 1F, age 30.2 ± 1.9 y/o) were included in these experiments. The imaging parameters were the same as in the previous CBF measurements, except that: TR/TE = 5 s/ 14.7 ms, the readout matrix = 48 × 48, 16 pairs of label and control following 2 dummy repetitions, no BGS. Note that the flow-crushing gradients with V_c = 2 cm/s along the S/I direction were necessary to remove intravascular signals, especially in the acquisitions with short TIs. The labeling parameters are listed below.

VSASL: VSASL-1VSS with V_c = 2 cm/s along the S/I direction, and TIs = [0.6, 1.2, 1.8, 2.4, 3.0, 3.6, 4.2] s.

PASL: PICORE without QUIPSS II, inversion slab thickness = 200 mm, a 20 mm gap between labeling and imaging slabs, and TIs = [0.6, 1.2, 1.8, 2.4, 3.0, 3.6, 4.2] s.

PCASL: The gaps between the labeling and imaging slabs were 47.2 ± 5.4 (mean ± STD) mm, label durations = [0.55, 1.15, 1.75, 1.75, 1.75, 1.75, 1.75] s at corresponding TIs = [0.6, 1.2, 1.8, 2.4, 3.0, 3.6, 4.2] s, with PLDs = [0.05, 0.05, 0.05, 0.65, 1.25, 1.85, 2.45] s. Note that instead of using one fixed (and small) value in all the scans, the label durations were adjusted at different TIs. This should improve the SNRs in the scans with long TIs while retaining the capability of detecting short TDs with ASL signals measured at short TIs.

High-resolution anatomical images were also collected to generate partial volume ratio maps of GM, WM and CSF, and GM ROIs.

The VSASL signals measured in multi-TI experiments were corrected for diffusion attenuation effects as done previously. The ASL signals collected with PASL, PCASL and VSASL were spatially smoothed by a 3×3 Gaussian kernel with a σ of 0.65, and then fitted to a kinetic ASL signal model (24) for the TDs and BDs per voxel. For the data collected with PCASL, only TD maps were calculated from the model with assumed BDs equal to the labeling durations used in the experiments. Note that in the process of fitting the VSASL data, the TDs were allowed to be negative, so the effects of noise and/or artifact that may shift the TDs to below zero can be observed. Fitted BDs associated with negative TDs were modified by $BD_{output} = BD_{fit} + TD_{negative}$, so the BDs in these voxels were correctly estimated. To minimize potential bias from noisy pixels, only the middle 95% (i.e., from 2.5% to 97.5%) of fitted TDs and BDs were analyzed. To demonstrate the goodness of the fits, R^2 maps were also calculated for each preparation method.

RESULTS

Simulations

Normalized SNR efficiencies of PASL and PCASL and VSASL are shown in Figure 3. The TI and TI_1/TI_2 used to reach the maximal SNR efficiencies in VSASL-1VSS and VSASL-2VSS at each TR are shown in Figure 3b and c respectively. The SNR efficiencies of VSASL using an unlimited BD and a BD of 2.0 s were identical. As shown in Figures 3b and 3c, a BD of 2.0 s is more than sufficient to achieve optimal SNR efficiencies at TR $\in$ [1, 8] s. Compared with VSASL-1VSS at the same TR, using 2 VSS modules improved the SNR efficiency by a minimal value of 18.1% at TR of 1 s and a maximal value of 26.0% at TR of 8 s. The maximal SNR efficiency of VSASL-1VSS was reached at TR = 4.9 s and TI = 1.4 s. The maximal SNR efficiency of VSASL-2VSS was reached at TR = 5.1 s and TI_1/TI_2 = 1.3 s/0.9 s, with an improvement of 24.4% compared to VSASL-1VSS. Potential CBF overestimation was estimated to be less than 7.6% with these imaging parameters and the P_1 values ranging from 0 to 0.5. However, adding the third VSS module only improved the SNR efficiency marginally, with an improvement of 26.9% compared to VSASL-1VSS (the dotted red line in Fig. 3a). This is because the ASL signal gain introduced by the third VSS module was mostly canceled by the additional attenuation from T_2 relaxation.

For PASL, the maximal SNR efficiency was reached when the TR was just long enough to include the designated BD, PLD and the imaging time. This is because the maximal ASL signal available is determined once the BD is fixed, so the maximal SNR efficiency will be achieved when the minimal TR (with minimal T_1 relaxation) is used: TR = 3.1 s with PLD = 1.5 s and TR = 3.6 s with PLD = 2 s. For PCASL, long TRs allow long labeling durations to be used, which increase ASL signals; however, the signal attenuation from T_1 relaxation is also increase as the image acquisition is delayed. So its maximal SNR efficiencies will be achieved when these two competing factors reach balance – in the simulation, they were achieved at TR = 5, 5.7 and 6.4 s with PLD = 1.5, 2 and 2.5 s accordingly.

VSASL was capable of acquiring ASL signal at very short TRs (< 2 s, Fig. 3a), where PASL and PCASL were typically not, due to the TD effect, unless the timing of labeling and acquisition is arranged so that the ASL signal acquired is from previous instead of current TR, e.g., as in (25). With a short TD/PLD (1.5 s), PCASL gave the highest SNR efficiency and VSASL-2VSS had higher SNR efficiency than PASL at TR > 4 s. For both PASL and PCASL, the SNR efficiencies were compromised when the PLD increased, due to increased T_1 relaxation. At PLD = 2 s, the SNR efficiency of PASL was the lowest among the three; while the SNR efficiency of VSASL-2VSS was higher than that of PCASL at TR < 4 s, but lower at TR > 4 s. At TD/PLD = 2.5 s, VSASL-1VSS gave comparable maximal SNR efficiency with PCASL, while VSASL-2VSS provided significantly higher SNR efficiency than PCASL.

CBF Measurements

The ASL signal and quantitative CBF maps of one representative slice calculated from PASL, PCASL, VSASL-1VSS, VSASL-2VSS and VSASL-2VSS-1BGS data are shown in Figure 4 for all the seven subjects. Averaged ASL and CBF values within the GM and WM

ROIs are reported in Table 1. GM/WM CBF ratios were also calculated. Pair-wise t-tests were performed on the ASL, CBF values and the GM/WM CBF ratios, and the *P*-values are tabulated in Table 2. Note that the significance detection level was set at 0.005 for the multiple comparisons with Bonferroni correction applied.

PASL had the lowest SNRs in both GM ($P \leq 6.6 \times 10^{-6}$) and WM ($P \leq 1.6 \times 10^{-4}$) ROIs among all the preparations. Compared with PCASL, VSASL-1VSS data had slightly lower (not significantly in GM with $P = 0.013$, but significantly in WM with $P = 5.1 \times 10^{-4}$). There was no significant difference between the SNR of the ASL signal measured by VSASL-2VSS and VSASL-2VSS-1BGS ($P = 0.38$ and 0.68 in GM and WM, respectively), so they were averaged together. Overall, VSASL-2VSS provided higher SNRs than PCASL, significantly so in GM ($P = 4.3 \times 10^{-3}$), though not significantly so in WM ($P = 0.46$). Compared with VSASL-1VSS, using two VSS modules significantly improved the SNRs in both GM (19.0 ± 2.2%, mean ± stand error of the mean (SEM), $P = 2.3 \times 10^{-4}$) and WM (25.2 ± 2.9%, $P = 7.1 \times 10^{-5}$). The averaged SNR gain over GM and WM was 22.1 ± 1.9% ($P = 1.7 \times 10^{-6}$), matched well with that of 22.7% predicted by simulation using the same preparation and imaging parameters. This validated our ASL signal model of using two VSS modules. In addition, the raw tissue signal levels were identical between VSASL-2VSS and VSASL-2VSS-1BGS scans (data not shown), indicating that the modified VSS module successfully served as a BGS pulse, with reduced overall SAR.

Averaged CBF values are listed in Table 1. Averaged GM/WM CBF ratio across subjects and the preparations was 2.37 ± 0.04 (mean ± SEM). All the GM and WM CBF values and GM/WM CBF ratios were in expected physiological range, and were consistent with the values reported in literatures (11,26,27). There was no significant difference between the GM/WM CBF ratios measured by different preparations, except between PCASL and VSASL-1VSS (Table 2), which could likely be caused by residual artifact from diffusion attenuation. The lowest CBF values in both GM and WM ROIs were reported by PASL, likely due to the compromised SNRs. However, only GM CBF values measured by PASL were significantly lower than that by VSASL-1VSS and VSASL-2VSS (Table 2). There was no other significant difference between the CBF values measured by different preparations tested, in GM or WM ROIs.

Multi-TI Experiments

Exemplary ASL signal maps acquired from the middle three slices in subject 5 using PASL, PCASL and VSASL at different TIs are shown in Figure 5a, with the averaged ASL signals in GM ROIs shown in Figure 5b. Corresponding TD, BD and R^2 maps are shown in Figure 5c (see supplementary material for results from the other 4 subjects). Note that due to relatively low SNRs and therefore compromised goodness of the fits in WM ROIs (see R^2 maps in Fig. 5c), only the TDs and BDs within the GM ROIs were analyzed, and their distributions are shown in Figure 5d. For both PCASL and PASL, the ASL signals in most GM regions were not detected at TI = 0.6 s, and delayed delivery of arterial blood in the posterior and territory boundary regions compared to other regions can be observed at later TIs, demonstrating the existence of TDs associated with these two labeling methods. The spatial distributions of TDs fitted from the PCASL and PASL data were consistent with each

other as expected, suggesting the validity of the fitting process. In contrast, VSASL did not show strong TD effects in the ASL images, and the fitted TDs in most of the GM were distributed around zero, as predicted by theory. However, the distribution was skewed towards negative values (Fig. 5d), likely due to contamination from residual diffusion attenuation and/or eddy current effects. The voxels with relatively large negative TDs were found mostly close to vessels or ventricles, suggesting possible presence of double-tagging effect (28). Both effects may artificially increase the ASL signal measured at short TIs, resulting in negative-biased TDs. The BDs measured by VSASL in this study were less likely to be affected by these contaminations, because 1) the two effects should have less impact on data collected at later TIs, especially that from the double-tagging effect (28); and 2) the increased portion in BDs due to negative TDs was removed (see Methods). The BDs measured in GM from the PASL and VSASL data were in a reasonable range, and those from the PASL data were consistent with values reported by others (29,30).

Means, medians and STDs of TDs and BDs in each slice are shown in Figure 6a and b for each subject. Note that due to the skewed distribution of TDs, the median instead of mean values should reflect the true values more accurately, therefore they are reported. For both PCASL and PASL, the TDs increased as the slice moved higher, because it takes more time for arterial blood to be delivered to more distal locations. On the other hand, the TDs using VSASL remained relatively constant and close to zero in all the slices, demonstrating the TD insensitivity of VSASL. PCASL showed longer TDs than PASL ($P = 4.4 \times 10^{-15}$), likely because the gaps between the labeling and imaging regions were bigger in PCASL than that in PASL (47.2 ± 5.4 mm vs. 20 mm). A Bland-Altman plot of the TDs measured using PCASL and PASL from different slices and subjects is shown in Figure 6c, with a mean difference of 0.23 s and a 95% confidence interval (CI) of [0.03, 0.43] s. The findings with regards to the TDs using PASL and PCASL were consistent with results reported in (31). The BDs measured using VSASL were significantly longer than that using PASL ($P = 5.2 \times 10^{-10}$). The BD difference was larger in higher slices, indicating the labeling of arterial blood within the imaging slab using VSASL, as expected. The Bland-Altman plot of the BDs measured using PASL and VSASL is shown in Figure 6d, with the mean difference and 95% CI being 0.64 s and [−0.23, 1.52] s, respectively.

The TDs and BDs averaged across slices are summarized in Table 3. Across the five subjects, the averaged TDs were (mean ± SEM): 1.16 ± 0.07 s, 0.93 ± 0.08 s and −0.09 ± 0.07 s for PCASL, PASL and VSASL respectively, and the averaged BDs were (mean ± SEM): 1.38 ± 0.09 s, 2.03 ± 0.08 s for PASL and VSASL respectively. Compared to PASL and PCASL, VSASL was indeed insensitive to TD effects as expected.

Discussion

The SNR improvement using two VSS modules was demonstrated through simulations and verified in in vivo experiments. The improvement can be explained by combination of bigger label/control difference created by re-saturation at later times, and lengthened effective BD. The former was demonstrated to be the dominant source of the SNR gain in this study. However, in practice, the latter may contribute significantly if the condition $TI_1 + TI_2 \leq BD$ is not met, e.g., if the BD is small due to limited coverage of a local RF coil and/or

fast bulk blood flow. The consistency of SNR improvements through simulations and in vivo experiments supports the validity of the mm-VSASL model.

As discussed in the Theory, the T_2 relaxation of VSS module affects the overall achievable SNR improvement using mm-VSASL: the less T_2 relaxation, the higher SNR improvement. In this study, sym-BIR-8 VSS modules were used to trade off some of the SNR gain for more accurate perfusion quantification with minimized eddy current effects; however, with the technical development in pulse design and/or hardware to further reduce eddy current effects, it may allow more efficient (less T_2 relaxation) and/or more number of VSS modules to be used to maximize the SNR efficiency gain. For instance, if the eTE is reduced to 10 ms for each VSS module, then the SNR efficiency improvement will be 33.5% and 45.5% for VSASL-2VSS and VSASL-3VSS respectively.

As demonstrated in both the simulations and the in vivo experiments, mm-VSASL was able to achieve SNR efficiencies that were significantly higher than PASL and comparable to PCASL with reasonable PLDs (~2 s, see Figs. 3 and 4, Table 1). In practice, slightly long/conservative PLDs (e.g., 2.5 s) may be considered using PCASL, even in healthy subjects, to accurately measure GM CBF without underestimation in some brain regions, as demonstrated in (26), where underestimation of GM CBF at border regions was observed in some subjects with PLD = 1.5 s compared to that with PLD = 2.5 s using PCASL. In cases of long TDs (e.g., ≥ 2.5 s), VSASL should be the best option among the three ASL categories with highest SNR efficiency and insensitivity to TD effects, or perhaps in the worst cases the only option if the TDs are so long that ASL signals are not practically detectable using PASL or PCASL.

Compared to PCASL, VSASL yielded slightly higher CBFs values, though not significantly so (Table 2). This may be explained by: 1) possible overestimation of CBF using VSASL caused by the residual artifact from the diffusion attenuation correction and/or eddy current effects, or unaccounted ASL signal from labeling of replenished arterial blood; or 2) possibly some regional perfusion underestimation using PCASL from compromised labeling efficiency due to off-resonance effects at the labeling planes, and/or TD sensitivity even with the relatively conservative PLDs used.

The data and fitted results of multi-TI experiments provided direct experimental evidence to demonstrate the TD insensitivity of VSASL. However, the artifact from eddy current and double-tagging effects might have contaminated the data, especially at early TI, resulting in slightly shifted TDs. Unreliable fitting results were seen in the WM regions in analysis of PCASL, PASL and VSASL data, where the SNR was relatively low. To accurately measure the TDs in the WM regions, high SNR data, e.g. with more repetitions or lower spatial resolution, are required.

Measured BDs validated that used in the PASL and VSASL simulations. For VSASL, a finite BD of 2 s, as measured in this study, is more than sufficient to achieve maximal SNR efficiency. There was no evidence that conventional VSASL had inaccurately quantified CBF due to the actual BD being shorter than the assumed value. On the other hand, mm-VSASL allows shorter BDs to be used for each VSS module to achieve the maximal SNR

efficiency at a given TR, so it should be even less likely to inaccurately quantify CBF if there is discrepancy between the actual and the assumed BD values.

Finally, there are also some potential concerns using mm-VSASL. First, as the VSS modules are applied more than once, it is possible that the artifacts from eddy current effects may be more profound, so caution must be taken, e.g., using VSS modules that are insensitive to eddy current effects. Second, as the diffusion attenuation correction is applied on each VSS module used, the more VSS modules used the less accurate the correction may be. Third, though there was no issue concerning SAR at 3 Tesla as in this study, there could be potential concerns at higher fields using multiple VSS modules.

Conclusions

It has been demonstrated through simulations and in vivo experiments that utilizing multiple VSS modules can increase the SNR efficiency of VSASL to levels comparable to or even higher than that of PCASL with reasonable PLDs. The TD insensitivity of VSASL, as experimentally verified in this study, also helps mm-VSASL provide perfusion quantification with improved accuracy. With these two advantages, mm-VSASL should be suitable in applications where long/heterogeneous TDs are of concern due to physiological or pathological reasons.

Supplementary Material

Refer to Web version on PubMed Central for supplementary material.

Acknowledgement

This work was funded by NIH R01 EB002096.

References

1. Kwong KK, Belliveau JW, Chesler DA, Goldberg IE, Weisskoff RM, Poncelet BP, Kennedy DN, Hoppel BE, Cohen MS, Turner R, Cheng H-M, Brady TJ, Rosen BR. Dynamic magnetic resonance imaging of human brain activity during primary sensory stimulation. Proc Natl Acad Sci USA. 1992; 89:5675–5679. [PubMed: 1608978]
2. Williams DS, Detre JA, Leigh JS, Koretsky AP. Magnetic resonance imaging of perfusion using spin inversion of arterial water. Proc Natl Acad Sci USA. 1992; 89:212–216. [PubMed: 1729691]
3. Edelman RR, Siewert B, Darby DG, Thangaraj V, Nobre AC, Mesulam MM, Warach S. Qualitative mapping of cerebral blood flow and functional localization with echo-planar MR imaging and signal targeting with alternating radio frequency (STAR) sequences: applications to MR angiography. Radiology. 1994; 192:513–520. [PubMed: 8029425]
4. Kim SG. Quantification of relative cerebral blood flow change by flow-sensitive alternating inversion recovery (FAIR) technique: application to functional mapping. Magn Reson Med. 1995; 34(3):293–301. [PubMed: 7500865]
5. Wong EC, Buxton RB, Frank LR. Implementation of quantitative perfusion imaging techniques for functional brain mapping using pulsed arterial spin labeling. NMR in Biomed. 1997; 10:237–249.
6. Dai WY, Garcia D, de Bazelaire C, Alsop DC. Continuous Flow-Driven Inversion for Arterial Spin Labeling Using Pulsed Radio Frequency and Gradient Fields. Magn Reson Med. 2008; 60(6):1488–1497. [PubMed: 19025913]

7. Alsop DC, Detre JA. Reduced transit-time sensitivity in noninvasive magnetic resonance imaging of human cerebral blood flow. J Cereb Blood Flow and Metab. 1996; 16:1236–1249. [PubMed: 8898697]
8. Ye FQ, Mattay VS, Jezzard P, Frank JA, Weinberger DR, McLaughlin AC. Correction for vascular artifcats in cerebral blood flow values measured by using arterial spin tagging techniques. Magn Res Med. 1997; 37:226–235.
9. Wong EC, Buxton RB, Frank LR. Quantitative imaging of perfusion using a single subtraction (QUIPSS and QUIPSS II). Magn Reson Med. 1998; 39(5):702–708. [PubMed: 9581600]
10. Wu WC, Wang J, Detre JA, Ratcliffe SJ, Floyd TF. Transit delay and flow quantification in muscle with continuous arterial spin labeling perfusion-MRI. J Magn Reson Imaging. 2008; 28(2):445–452. [PubMed: 18666182]
11. van Osch MJP, Teeuwisse WM, van Walderveen MAA, Hendrikse J, Kies DA, van Buchem MA. Can arterial spin labeling detect white matter perfusion signal? Magn Reson Med. 2009; 62(1): 165–173. [PubMed: 19365865]
12. Bokkers RPH, Bremmer JP, van Berckel BNM, Lammertsma AA, Hendrikse J, Pluim JPW, Kappelle LJ, Boellaard R, Klijn CJM. Arterial spin labeling perfusion MRI at multiple delay times: a correlative study with (H2O)-O-15 positron emission tomography in patients with symptomatic carotid artery occlusion. J Cereb Blood Flow Metab. 2010; 30(1):222–229. [PubMed: 19809464]
13. Yun TJ, Sohn CH, Han MH, Kang HS, Kim JE, Yoon BW, Paeng JC, Choi SH, Kim JH, Song IC, Chang KH. Effect of delayed transit time on arterial spin labeling: correlation with dynamic susceptibility contrast perfusion magnetic resonance in moyamoya disease. Invest Radiol. 2013; 48(11):795–802. [PubMed: 23764569]
14. Wong, EC.; Liu, T.; Sidaros, K.; Frank, LR.; Buxton, RB. Velocity selective arterial spin labeling. Proceedings of the 10 th Annual Meeting of ISMRM; Honolulu, Hawai'i, USA. 2002. p. 621
15. Duhamel G, de Bazelaire C, Alsop DC. Evaluation of systematic quantification errors in velocity-selective arterial spin labeling of the brain. Magn Reson Med. 2003; 50(1):145–153. [PubMed: 12815689]
16. Wong EC, Cronin M, Wu W-C, Inglis B, Frank LR, Liu TT. Velocity-selective arterial spin labeling. Magn Reson Med. 2006; 55(6):1334–1341. [PubMed: 16700025]
17. Wu W-C, Fernández-Seara M, Detre JA, Wehrli FW, Wang J. A theoretical and experimental investigation of the tagging efficiency of pseudocontinuous arterial spin labeling. Magn Reson Med. 2007; 58(5):1020–1027. [PubMed: 17969096]
18. Guo J, Meakin JA, Jezzard P, Wong EC. An optimized design to reduce eddy current sensitivity in velocity-selective arterial spin labeling using symmetric BIR-8 pulses. Magn Reson Med. 2014 doi: 10.1002/mrm.25227.
19. Ye FQ, Frank JA, Weinberger DR, McLaughlin AC. Noise reduction in 3D perfusion imaging by attenuating the static signal in arterial spin tagging (ASSIST). Magn Reson Med. 2000; 44(1):92–100. [PubMed: 10893526]
20. Zun Z, Hargreaves BA, Pauly J, Zaharchuk G. Near-contiguous spin echo imaging using matched-phase RF and its application in velocity-selective arterial spin labeling. Magn Reson Med. 2014; 71(6):2043–2050. [PubMed: 23857667]
21. Cox RW. AFNI: software for analysis and visualization of functional magnetic resonance neuroimages. Comput Biomed Res. 1996; 29(3):162–173. [PubMed: 8812068]
22. Kuroiwa T, Nagaoka T, Ueki M, Yamada I, Miyasaka N, Akimoto H. Different apparent diffusion coefficient: water content correlations of gray and white matter during early ischemia. Stroke. 1998; 29(4):859–865. [PubMed: 9550523]
23. Le Bihan D, Turner R, Douek P, Patronas N. Diffusion MR imaging: clinical applications. AJR Am J Roentgenol. 1992; 159(3):591–599. [PubMed: 1503032]
24. Buxton RB, Frank LR, Wong EC, Siewert B, Warach S, Edelman RR. A general kinetic model for quantitative perfusion imaging with arterial spin labeling. Magn Reson Med. 1998; 40:383–396. [PubMed: 9727941]
25. Wong EC, Luh WM, Liu TT. Turbo ASL: Arterial Spin Labeling with Higher SNR and Temporal Resolution. Magn Reson Med. 2000; 44(4):511–515. [PubMed: 11025504]

26. Wu B, Lou X, Wu X, Ma L. Intra- and interscanner reliability and reproducibility of 3D whole-brain pseudo-continuous arterial spin-labeling MR perfusion at 3T. J Magn Reson Imaging. 2014; 39(2):402–409. [PubMed: 23723043]

27. Wang J, Alsop DC, Li L, Listerud J, Gonzalez-At JB, Schnall MD, Detre JA. Comparison of quantitative perfusion imaging using arterial spin labeling at 1.5 and 4.0 Tesla. Magn Reson Med. 2002; 48(2):242–254. [PubMed: 12210932]

28. Gallichan, D.; Jezzard, P. Simulating the tagging process in velocity-selective ASL. Proceedings of the 15 th Annual Meeting of ISMRM; Berlin, Germany. 2007. p. 3488

29. Villien M, Chipon E, Tropres I, Bouvier J, Cantin S, Chechin D, Le Bas JF, Krainik A, Warnking JM. Per-subject characterization of bolus width in pulsed arterial spin labeling using bolus turbo sampling. Magn Reson Med. 2013; 69(6):1677–1682. [PubMed: 22829470]

30. Hales PW, Kawadler JM, Aylett SE, Kirkham FJ, Clark CA. Arterial spin labeling characterization of cerebral perfusion during normal maturation from late childhood into adulthood: normal 'reference range' values and their use in clinical studies. J Cereb Blood Flow Metab. 2014; 34(5): 776–784. [PubMed: 24496173]

31. Cavusoglu M, Pohmann R, Burger HC, Uludag K. Regional effects of magnetization dispersion on quantitative perfusion imaging for pulsed and continuous arterial spin labeling. Magn Reson Med. 2013; 69(2):524–530. [PubMed: 22488815]

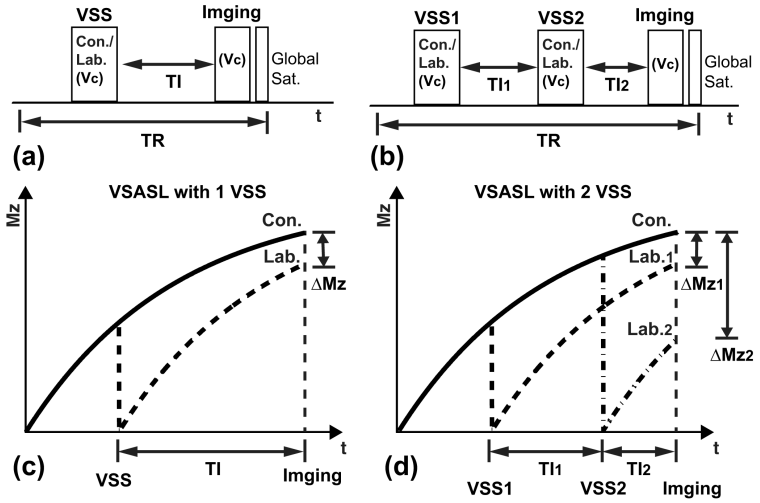

FIG. 1.

Sequence diagrams and Schematic description of conventional VSASL (a, c), and VSASL using two VSS modules (b, d). In c and d, the solid curves represent the magnetization of arterial blood under control condition. The dashed curve in (c) represents the magnetization of arterial blood under label condition. The dashed curve in (d) represents the magnetization of arterial blood that is labeled only by the first VSS module. The dot-dashed curve in (d) represents the magnetization of arterial blood that is labeled only by the second VSS module. The magnetization of arterial blood that is labeled by both VSS modules follows the dashed curve before and the dot-dashed curve after the application of the second VSS module.

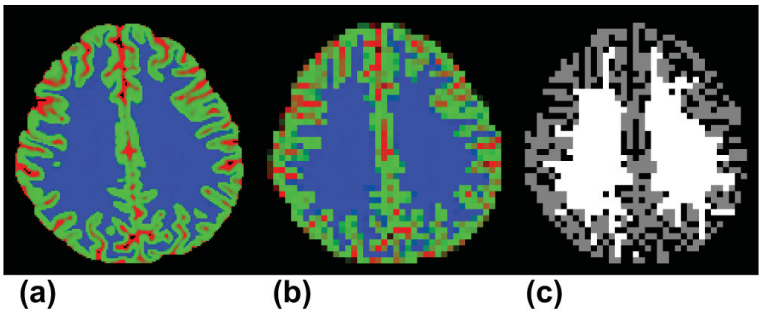

FIG. 2.

Examples of partial volume maps (GM in green, WM in blue and CSF in red) at high (a) and low (b) resolutions, and generated GM and WM ROIs (c, GM in gray, WM in white).

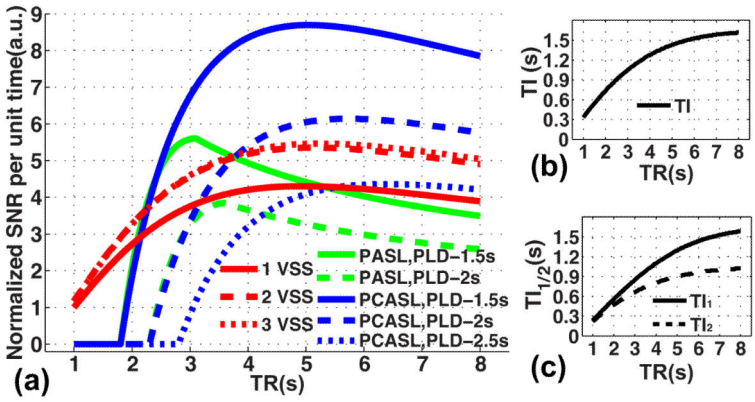

FIG. 3.

Simulation results showing the maximal SNR efficiencies using different ASL preparations at given TRs (a), and the TIs to achieve the maximal SNR efficiencies using VSASL with one (b) or two (c) VSS modules. SNR efficiencies of VSASL with one, two or three VSS modules are depicted with solid, dashed and dotted red curves respectively. SNR efficiencies of PASL with PLDs of 1.5 s and 2 s are depicted with solid and dashed green curves respectively. SNR efficiencies of PCASL with PLDs of 1.5 s, 2 s and 2.5 s are depicted with solid, dashed and dotted blue curves respectively.

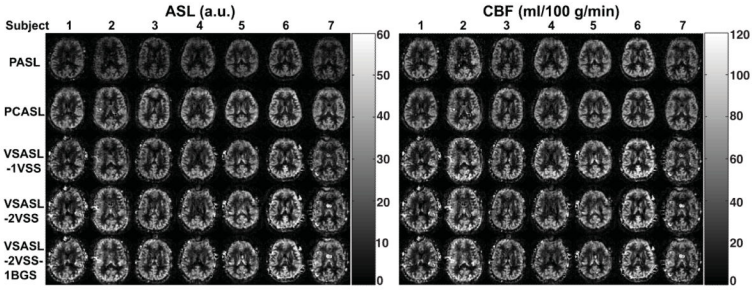

FIG. 4.

Examples of ASL (left panel) and quantitative CBF (right panel) maps measured with different preparations for all the seven subjects (only one slice is shown). The rows of maps from top to bottom were acquired with PASL, PCASL, VSASL-1VSS, VSASL-2VSS and VSASL-2VSS-1BGS respectively.

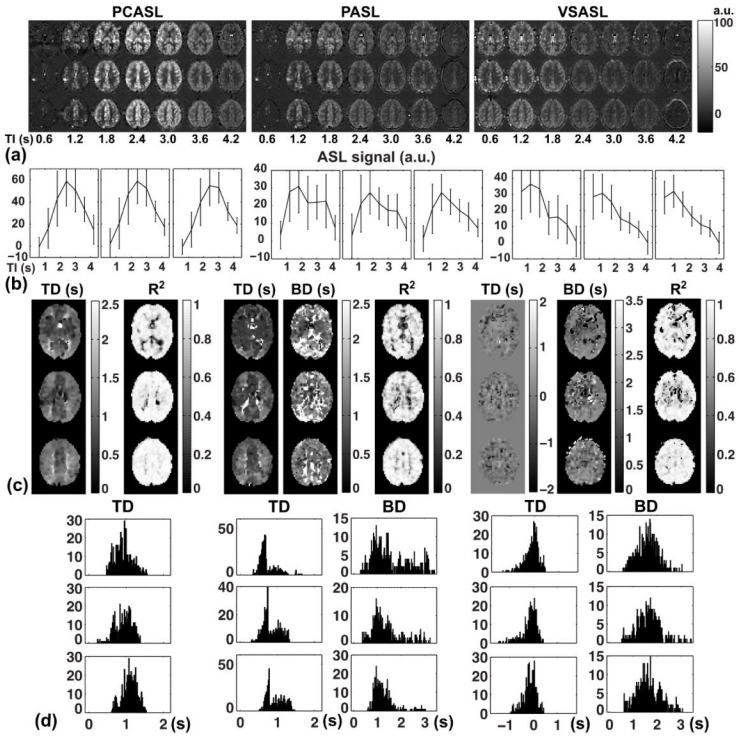

FIG. 5.

Examples of the data and fitted results from the multi-TI experiments on subject 5: (a) ASL images acquired at different TIs using PCASL (left), PASL (middle) and VSASL (right), three slices shown at different rows; (b) averaged ASL signals in GM ROIs at different TIs; (c) fitted TD, BD and R^2 maps from (a), note the similar patterns between the TD maps using PCASL and PASL, and the nearly-zero TDs in most regions using VSASL; (d) the histograms of TDs and BDs within the GM ROIs.

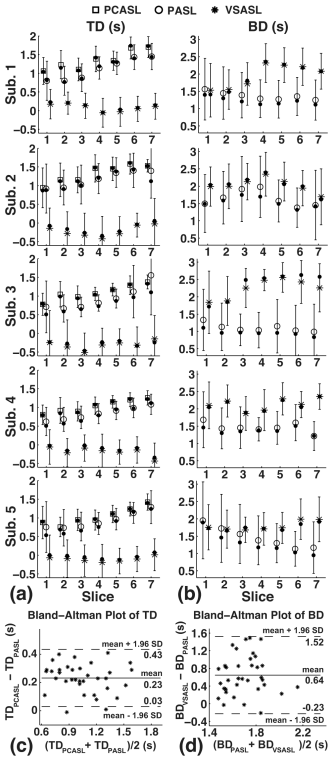

FIG. 6.

Means and STDs of TDs (a) and BDs (b) in each slice measured using PCASL (square), PASL (circle) and VSASL (star) for each subject, where the dots on the error bars represent the median values; (c) the Bland-Altman plot of TDs measured with PCASL and PASL, showing the TD difference between the two; (d) the Bland-Altman plot of BDs measured with PASL and VSASL, showing BD difference between the two.

Table 1

Averaged ASL signals (a.u.), CBF values (mean ± tSTD, unit ml/min/100 g) across GM and WM ROIs and GM/WM (G/W) ratios for each subject and across subjects (mean ± SEM).

	Sequence	PASL		PCASL		VSASL-1VSS		VSASL-2VSS		VSASL-2VSS-1BGS	
Subject	**ROI**	**GM**	**WM**	**GM**	**WM**	**GM**	**WM**	**GM**	**WM**	**GM**	**WM**
1	ASL	15.6	7.6	23.9	12.0	21.5	8.7	25.7	10.9	26.6	11.6
	CBF	45.7 ± 3.5	21.6 ± 2.1	46.1 ± 5.1	22.5 ± 2.3	50.3 ± 4.1	20.4 ± 2.6	49.1 ± 7.2	21.0 ± 4.2	49.3 ± 5.0	21.6 ± 3.4
	G/W Ratio	2.11		2.04		2.47		2.34		2.29	
2	ASL	11.3	5.1	19.6	9.0	18.7	7.8	23.2	10.5	24.3	10.9
	CBF	42.9 ± 14.4	19.0 ± 6.0	49.2 ± 8.6	22.0 ± 4.1	56.9 ± 8.4	23.7 ± 4.1	57.5 ± 12.9	26.1 ± 6.2	58.5 ± 8.5	26.2 ± 4.1
	G/W Ratio	2.26		2.23		2.40		2.20		2.24	
3	ASL	13.6	5.1	24.5	9.6	21.0	7.3	25.3	9.6	25.8	9.8
	CBF	40.0 ± 1.9	14.8 ± 1.5	47.4 ± 5.6	18.3 ± 2.7	49.6 ± 6.3	17.3 ± 3.3	48.8 ± 6.8	18.4 ± 3.8	48.2 ± 5.1	18.3 ± 2.8
	G/W Ratio	2.69		2.59		2.86		2.65		2.64	
4	ASL	15.8	7.4	24.4	12.6	25.1	11.1	26.6	12.5	26.3	12.0
	CBF	48.9 ± 4.4	22.2 ± 2.1	49.6 ± 7.0	24.7 ± 3.4	61.7 ± 9.7	27.4 ± 5.4	53.4 ± 9.7	25.2 ± 6.8	51.2 ± 9.1	23.4 ± 5.8
	G/W Ratio	2.20		2.01		2.25		2.12		2.19	
5	ASL	17.3	7.9	27.9	12.5	25.8	10.6	30.1	13.8	27.8	12.1
	CBF	50.4 ± 3.8	22.5 ± 2.1	53.2 ± 6.4	23.4 ± 4.7	59.9 ± 4.9	24.7 ± 3.5	57.2 ± 5.2	26.2 ± 5.3	51.2 ± 3.3	22.3 ± 4.1
	G/W Ratio	2.24		2.27		2.42		2.18		2.29	
6	ASL	16.9	6.9	28.3	10.5	26.4	9.3	31.3	10.8	32.4	11.0
	CBF	53.4 ± 6.0	21.4 ± 2.1	58.7 ± 9.7	21.4 ± 5.9	66.6 ± 10.4	23.5 ± 4.7	64.5 ± 6.0	22.3 ± 4.3	64.7 ± 9.4	22.1 ± 8.1
	G/W Ratio	2.49		2.74		2.84		2.89		2.93	
7	ASL	12.2	5.8	22.2	10.5	18.6	8.4	21.5	9.7	24.7	11.8
	CBF	36.0 ± 2.7	16.6 ± 1.5	42.8 ± 7.5	20.0 ± 4.6	43.8 ± 7.2	19.9 ± 4.5	41.2 ± 5.1	18.7 ± 3.0	46.0 ± 7.0	22.0 ± 4.4
	G/W Ratio	2.16		2.14		2.20		2.20		2.09	
Average	ASL	14.7 ± 0.9	6.5 ± 0.5	24.4 ± 1.1	11.0 ± 0.5	22.4 ± 1.2	9.0 ± 0.5	26.3 ± 1.3	11.1 ± 0.6	26.9 ± 1.0	11.3 ± 0.3
	CBF	45.3 ± 2.3	19.8 ± 1.1	49.6 ± 1.9	21.8 ± 0.8	55.5 ± 3.0	22.4 ± 1.3	53.1 ± 2.9	22.6 ± 1.3	52.7 ± 2.5	22.3 ± 0.9
	G/W Ratio	2.31 ± 0.08		2.29 ± 0.10		2.49 ± 0.10		2.37 ± 0.11		2.38 ± 0.11	

Table 2

The *P*-values of the pair-wise t-tests on ASL signal, CBF values within the GM and WM ROIs and corresponding G/W ratios using PASL, PCASL, VSASL-1VSS, VSASL-2VSS and VSASL-2VSS-1BGS. The *P*-values reached significance are labeled by "*" ($P < 0.005$, with Bonferroni correction applied).

			PCASL	**VSASL-1VSS**	**VSASL-2VSS**	**VSASL-2VSS-1BGS**
ASL	GM	PASL	1.1×10^{-6} *	6.6×10^{-6} *	2.2×10^{-6} *	1.8×10^{-6} *
		PCASL		0.013	0.014	7.0×10^{-3}
		VSASL-1VSS			1.5×10^{-4} *	1.0×10^{-3} *
		VSASL-2VSS				0.38
	WM	PASL	5.3×10^{-7} *	1.6×10^{-4} *	1.2×10^{-5} *	5.1×10^{-6} *
		PCASL		5.1×10^{-4} *	0.71	0.39
		VSASL-1VSS			2.3×10^{-4} *	6.3×10^{-4} *
		VSASL-2VSS				0.68
CBF	GM	PASL	8.8×10^{-3}	2.0×10^{-4} *	2.1×10^{-3} *	0.011
		PCASL		6.0×10^{-3}	0.024	0.062
		VSASL-1VSS			0.060	0.18
		VSASL-2VSS				0.79
	WM	PASL	9.4×10^{-3}	0.016	0.02	0.063
		PCASL		0.37	0.34	0.54
		VSASL-1VSS			0.82	0.88
		VSASL-2VSS				0.72
G/W Ratio		PASL	0.73	0.0079	0.42	0.33
		PCASL		0.0047 *	0.15	0.075
		VSASL-1VSS			0.026	0.031
		VSASL-2VSS				0.68

Table 3

Averaged TDs and BDs using PCASL, PASL and VSASL across GM ROIs in each subject (mean ± SEM, unit s).

Sequence	PCASL	PASL		VSASL	
Subject	**TD**	**TD**	**BD**	**TD**	**BD**
1	1.35 ± 0.11	1.11 ± 0.11	1.34 ± 0.04	0.11 ± 0.04	1.94 ± 0.13
2	1.31 ± 0.10	1.13 ± 0.08	1.62 ± 0.09	−0.15 ± 0.05	2.03 ± 0.08
3	1.08 ± 0.08	0.77 ± 0.08	1.06 ± 0.05	−0.28 ± 0.03	2.25 ± 0.11
4	1.03 ± 0.07	0.79 ± 0.09	1.44 ± 0.06	−0.12 ± 0.04	2.13 ± 0.07
5	1.03 ± 0.09	0.84 ± 0.11	1.44 ± 0.12	−0.03 ± 0.03	1.78 ± 0.05
Average	1.16 ± 0.07	0.93 ± 0.08	1.38 ± 0.09	−0.09 ± 0.07	2.03 ± 0.08